




Received 31 January 2023; revised 15 March 2023; accepted 17 March 2023.

Digital Object Identifier 10.1109/JMW.2023.3259990

Solid-State Power Combining for Heating Small Volumes of Mixed Waste Materials

MEGAN C. ROBINSON ¹ (Student Member, IEEE), JACK A. MOLLES ¹ (Student Member, IEEE),
VADIM V. YAKOVLEV ² (Senior Member, IEEE), AND ZOYA POPOVIĆ¹ (Fellow, IEEE)

(Regular Paper)

¹Department of Electrical, Computer, and Energy Engineering, University of Colorado Boulder, Boulder, CO 80309 USA

²Worcester Polytechnic Institute, Worcester, MA 01609 USA

CORRESPONDING AUTHOR: Megan C. Robinson (e-mail: megan.robinson@colorado.edu).

This work was supported by DARPA under Grant W911NF-18-1-0073.

ABSTRACT Microwave heating of waste results in chemical breakdown that can lead to conversion of mixed waste materials to fuel. Heating waste mixtures with microwave energy rather than incineration results in faster breakdown and can therefore be more efficient. Here we address heating of small volumes of mixed food waste materials with widely differing and temperature-dependent electrical properties. Uniform heating is accomplished with mode mixing within a loaded cavity and by spatial power combining of solid-state power amplifiers (SSPAs). We present a heating comparison of two circuit-combined and spatially-combined 2.45 GHz 70-W 65% efficient GaN SSPAs with controlled relative phase. The heating efficacy is shown to improve by volumetric combining inside the waste loading. The temperature changes in several locations and for several common waste materials and mixtures are investigated and compared to FEM electromagnetic simulations, as well as FDTD multi-physics simulations that incorporate thermal dependence of material properties. The approach is scalable in volume and power, demonstrated by a simulation comparison of the 1.4 L small cavity to a 5.2 L volume.

INDEX TERMS Microwave heating, power amplifiers, efficiency, power combining, multi-physics modelling.

I. INTRODUCTION

In 2017, the United States produced 243 million metric tons of waste, equivalent to 1.8 kg per person per day. Over half of the waste, 126.6 million tons, went into landfills and roughly 35%, 86 million tons, were recycled or composted [1]. Excess waste is becoming a global problem, as many countries are running out of landfill space and low-quality plastic is often sent back from recycling plants [2], [3]. In addition, the current waste-management systems are not taking full advantage of energy resources contained in the waste. Thermochemical processes, pyrolysis, incineration, gasification, etc., are currently used for energy production from waste material. Incineration and gasification directly use the material breakdown to generate electricity [4]. Pyrolysis does not directly process the waste for energy production, but converts it into intermediary compounds that can be used for chemical up-conversion to solid fuel, oil, SynGas [5], or environmentally safe products for e.g. fertilization [6].

Pyrolysis is defined as “the thermochemical decomposition of organic material at high temperature and in the absence of oxygen or in an atmosphere of inert gases” [7]. It has been investigated for feasibility in the municipal solid waste (MSW) sector, where convection-based heating methods for a wide variety of materials have been used, e.g. wood [8], paper [9], textiles [10], mixed food [11], and plastics [12]. These materials are the majority of MSW in most areas and are therefore the main topic of research. Most published experiments use non-renewable energy sources, or do not mention the energy usage of the heating apparatus. Limited work with microwave heating has shown improvement in thermal efficiency, increased speed of reactions, and, in some cases, advantageous modifications of the breakdown process [13]. Electromagnetic waves generate heat inside the medium, improving the system efficiency by reducing the amount of heat dissipated outside of the waste material compared to convection heating. Microwave heating has been shown to be much

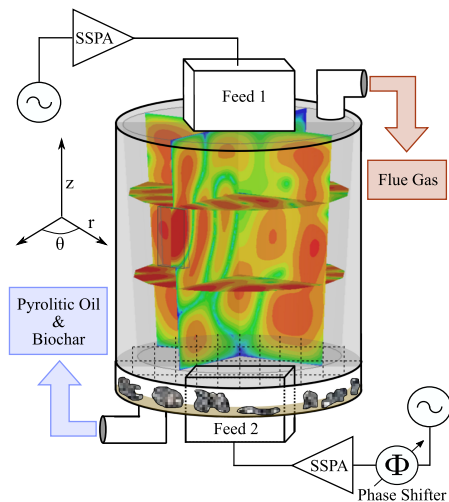


FIGURE 1. Diagram of microwave heating reactor fed by two solid-state power amplifiers (SSPAs) spatially combined in an overmoded cylindrical cavity loaded with mixed waste, with an example relative electric field magnitude shown in a few cross-sections. The phase shift ϕ is adjusted for improved heating uniformity. As a result of the pyrolysis process, coal, pyrolytic oil and gas can be obtained.

faster than conventional electric heating in hydrothermal treatments [14].

This paper describes a 2.45-GHz active microwave cavity with solid-state (GaN) spatially power-combined sources for scalable waste volumes, as illustrated in Fig. 1. Most microwave industrial heating is done with magnetrons with kW to MW power levels in the 915 MHz and 2.4 GHz ISM bands. However, the frequency is not easily tunable nor are multiple magnetrons easily injection-locked for power combining [15]. Small and even hand-held solid-state microwave ovens using LDMOS devices have been demonstrated [16]. A LDMOS solid-state source with 180 W of effective power and with frequency modulation is shown in [17] to help heating uniformity of chicken in both simulation and experiment. Here, we compare two 70 W GaN SSPPA excitations of a 1.4ℓ cylindrical cavity to a single 140 W excitation to assess the benefits of spatial power combining in the waste volume. Cardboard/paper, bread, meat (hotdog) and their mixtures are used as representative materials, chosen for the large range of complex dielectric constants. The approach is scalable and is first demonstrated on a small-volume 1.4ℓ personal “trashcan,” with measurements and simulations at temperatures below phase change. Additionally, a path towards scaling is shown on a 5.2ℓ model volume. Note that in the results presented here, we assume that the heating rate and material properties do not change drastically, i.e. that the heating is below phase change and the impedance of the cavity loading does not change dramatically. The two main reasons for conducting measurements at temperatures below phase change are: (1) the material properties, and by extension, the heating equation remains simpler and more reliable, without a need for chemical analysis; and (2) a fume hood for containing hazardous gases resulting from phase change is not available in the experimental setup. A substantial change in material properties due to

heating would also result in nonuniform material properties, and considering different permittivity mixtures can give an idea of the impact of nonuniformities from an electrical standpoint, but the variation in thermal properties are not explored.

The paper is organized as follows. Section II provides background related to microwave heating and waste electrical properties. Section III covers the cavity simulations and investigates the power density throughout uniform waste loadings as the relative phase between the sources is varied. Section IV describes several measurement setups as well as multi-physics simulations. Section V details measurements of heating for uniform waste loadings and compares with multi-physics simulations. Section VI extends the measurements to non-uniform waste mixtures, using several types of cavity feeding. Finally, the last section summarizes the most relevant conclusions and shows preliminary results for frequency-modulated cavity excitation and scaling to a larger cavity volume.

II. MICROWAVE HEATING THEORY

Heating materials with electromagnetic waves at microwave frequencies is a result of absorption in the material due to its high-frequency conductivity, σ . For example, a 100 mL volume of uniform material with $\sigma = 5$ S/m and specific heat of $c = 3.899$ J/g (salt water), exposed uniformly to 163 W of microwave power will heat by 75 K in 3 minutes. Heating is usually performed in a shielded metal cavity which is larger than a wavelength in each dimension, at one of the Industrial, Scientific and Medical (ISM) frequencies of 2.45 GHz or 915 MHz. Such a loaded electrically-large cavity is over-moded, implying that the electromagnetic field distribution is complicated and not uniform. The heating rate and temperature distribution depend on modes that are excited in the cavity, which in turn depend on frequency and both the real and imaginary parts of the complex permittivity, $\epsilon = \epsilon' - j\epsilon'' = \epsilon_0\epsilon_r - j\sigma/\omega$. We assume here that the waste loads the cavity fully and that waste materials are considered to be lossy dielectrics with a real-valued conductivity. The standard skin depth for a plane wave can be used as a guideline for penetration depth of the field into a given material, but in an over-moded cavity filled with a lossy material, full-wave simulations are needed to determine the field strength within the volume, and should be coupled with thermal simulations which include temperature-dependent material properties.

A. ELECTRICAL AND THERMAL PROPERTIES OF SOME WASTE MATERIALS

Electrical and thermal properties of typical waste materials at 2.45 GHz and 25 °C are given in Table 1, showing the large variation in permittivity, conductivity, specific heat, mass density, ρ , and thermal conductivity, κ . The bold-faced quantities are used in this work for the simulations and experiments.

Heat conservation within the cavity can be written as:

$$\frac{d\mathcal{E}_{\text{TH}}}{dt} = -\nabla \cdot \vec{\Phi}_{\text{H}} + Q, \quad (1)$$

TABLE 1. Table of Material Properties [18], [19], [20], [21], [22], [23], [24], [25], [26], [27]

Material	ϵ_r	σ [$\frac{mS}{m}$]	c [$\frac{kJ}{Kkg}$]	ρ [$\frac{kg}{m^3}$]	κ [$\frac{W}{Km}$]
Wood	1.2–2.1	4.9–8.6	1.3–2.4	400–750	0.15–0.19
Starches	30	2042	3.7	1050	1
Fruit & Veg.	4.6	31.3	3.8–4.1	840–1320	0.3–0.7
Plastics	2–3.5	1.3–2.4	1.3–1.9	540–800	0.03–0.5
Textiles	1.4–6	3.8–16.3	1.6	560	0.03–0.25
Paper	2–3	10.2	1.336	80–190	0.05
Bread	3.1–4.2	40–105	4.5	200	0.1
Meat	50–65	2–2.6k	2.7–3.7	960–1060	0.4–0.5

where Q is the energy of heat, $\vec{\Phi}_H$ is the heat flux vector and the thermal energy, \mathcal{E}_{TH} , is given by

$$\mathcal{E}_{TH} = c(r, \phi, z, T)\rho(r, \phi, z, T)T(t) + C. \quad (2)$$

Other energy stored in the material is absorbed into the constant C in (2). Cylindrical coordinates are used to match the experimental cavity geometry. Here we assume that the materials do not undergo phase or chemical changes over the temperature range considered ($\partial C/\partial t = 0$), and that the heat flux is caused by conduction only and is described by Fourier's law for an isotropic medium:

$$\vec{\Phi}_H = -\kappa(r, \phi, z, T)\nabla T. \quad (3)$$

The heat generation, Q , comes from Joule losses, with a power density at any point in the waste volume given by:

$$Q = p_J(r, \phi, z, T) = |\vec{E}(r, \phi, z, T)|^2\sigma(r, \phi, z, T), \quad (4)$$

where $\vec{E}(r, \phi, z)$ is the electric field, and $\sigma(r, \phi, z)$ is the spatially-varying conductivity. From (1), solving for the temperature increase gives:

$$\frac{\partial}{\partial t}T(r, \phi, z) = \frac{p_J(r, \phi, z, T) + \nabla \cdot (\kappa(r, \phi, z, T)\nabla T(r, \phi, z))}{\rho(r, \phi, z, T)c(r, \phi, z, T)}. \quad (5)$$

To solve these equations numerically, the composition and spatial variation of the mixed waste needs to be known. Even for a single material, the moisture content and density will vary. To compare measurements to theory, single-material cavity loading is first investigated, with cardboard/paper, bread and meat (hotdog). The CAD tool QuickWave [28] numerically implements equations (1)–(5) and is used to compare with experiments in Section IV-B.

III. MICROWAVE CAVITY SIMULATIONS

A 1.4ℓ shorted metal cylinder with a base diameter of 12.5 cm and height of 11.2 cm is used as the heating cavity, and completely filled with representative waste material. Two rectangular waveguide probes are placed symmetrically on the two cavity ends. This arrangement gives the option of relative feed rotation. At 2.45 GHz, the cavity is single-moded

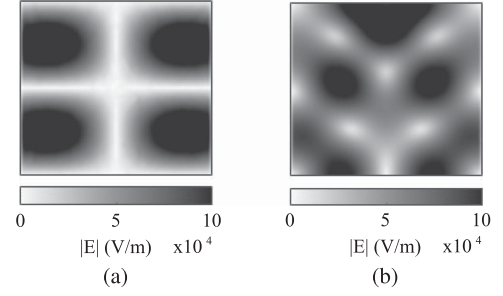


FIGURE 2. (a) Eigenmode simulations for the electric field magnitude in a cylindrical cavity with a diameter of 12.5 cm and height of 11.2 cm, loaded with paper, showing the single mode closest to 2.45 GHz normalized to 1 J of stored energy. (b) Driven simulation for the electric field magnitude in the cavity for a single WR340 rectangular waveguide probe excited with 70 W delivered power. Results for the central cross-section of the cylindrical cavity are shown.

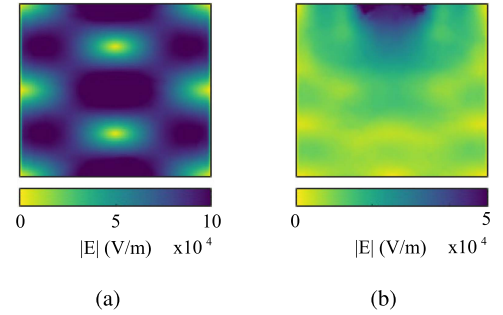


FIGURE 3. (a) Eigenmode simulations for the electric field magnitude in a cylindrical cavity with a diameter of 12.5 cm and height of 11.2 cm, loaded with bread, showing the single mode closest to 2.45 GHz normalized to 1 J of stored energy. (b) Driven simulation for the electric field magnitude in the cavity for a single rectangular waveguide probe with 70 W delivered power. Results for the central cross-section of the cylindrical cavity are shown.

when air-filled, but supports 3, 5 and more than 20 modes with uniform paper, bread and meat loading, respectively. The field amplitudes from eigenmode (unfed) analysis using Ansys HFSS are given in Fig. 2(a) for paper and in Fig. 3(a) for bread, showing the mode that is closest (within 250 MHz) to 2.45 GHz. The plots show the vertical cross-section of the cylindrical cavity ($r = -6.25$ to 6.25 cm, $z = 0$ to 11.2 cm). As expected, the field profiles are quite different for the two loadings.

A driven analysis with a single S-band (WR340) waveguide-to-coaxial adaptor feed is performed for all three uniform loadings, showing that multiple modes are present. The results for paper are shown in Fig. 2(b), for bread in Fig. 3(b), and for meat loading in Fig. 4. In all three cases, the highest field values are near the feed, but in the case of the lower-conductivity paper the field is more uniformly distributed throughout the volume. As expected, increased loss occurs near the feed for the most conductive loading (meat), with several orders of magnitude lower field at the opposite side of the cavity. From these plots, the motivation for including multiple feeds becomes obvious.

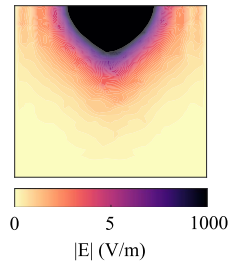


FIGURE 4. Driven simulation for the electric field magnitude in the cavity loaded with meat for a single waveguide probe excited with 70 W delivered power. Results for the central cross-section of the loaded cylindrical cavity are shown.

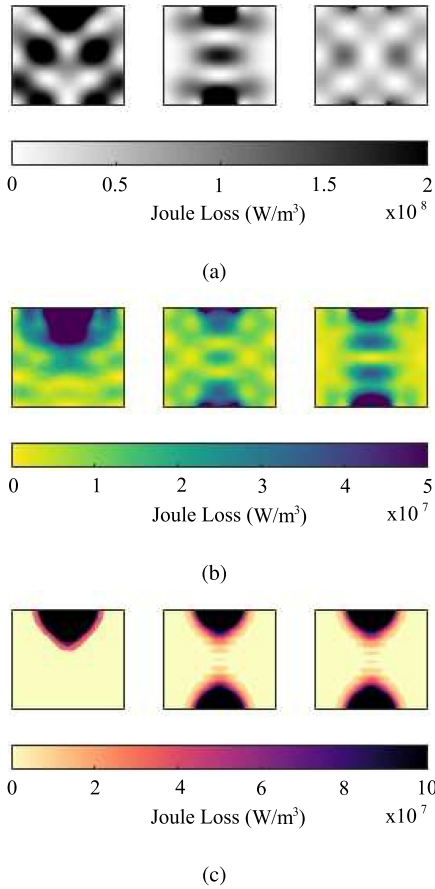


FIGURE 5. Driven simulation for the Joule loss in the cavity for uniform bread loading and different excitations. Left: Single waveguide probe excited with 70 W delivered power. Center: Two waveguide probes driven in phase with half of the applied power per probe. Right: Two waveguide probes driven 180° out of phase with half of the applied power per probe, for (a) paper, (b) bread, and (c) meat loadings. In all plots, results for the central cross-section of the loaded cylindrical cavity are shown.

From (4), the Joule loss density in the materials is proportional to the square of the field magnitude and the conductivity. It is interesting and practically relevant to note that the loss density is more uniform across different materials than the electric field magnitude. Fig. 5 shows simulation results using a driven analysis in HFSS for three excitations: two circuit-combined PAs feeding a single waveguide probe;

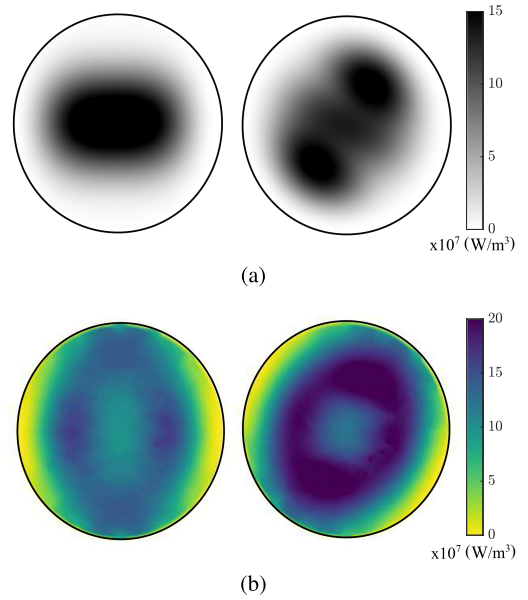


FIGURE 6. Joule loss volume energy density in the horizontal middle cross-section for (a) paper and (b) bread uniform loading with two feeds oriented parallel (left) and 45° (right) to each other for 70 W of total delivered power.

two probes fed by two PAs in phase; and two probes fed by two PAs out of phase. The loss power density distribution is affected dramatically for the paper and bread loadings, but not for the highly conductive meat loading.

It is interesting to visualize the electric fields in the middle horizontal cut of the cavity ($z = 5.6$ cm, $r = 0$ to 6.25 cm, $\theta = 0$ to 2π). The two feeds can be oriented parallel to each other, or at some angle. Fig. 6 shows the Joule loss density for paper and bread loading, for the parallel and 45° feed orientation. Although the 45° orientation results in a higher nonuniformity, the produced heat is significantly higher for both loadings.

IV. TEMPERATURE EVOLUTION

The above simulations show steady-state electric field and Joule losses for uniformly-filled cavities with a single or dual feed. When the power is turned on, heating will occur starting from these initial conditions. Due to thermal conduction and changes of material electrical and thermal properties with temperature, the electric field distribution will vary in time as heating continues. We next describe the experimental setup used to measure the temperature distribution over time, as well as multi-physics modeling that takes into account temperature-dependent material parameters. This enables a comparison of measured and simulated temperature evolution over time.

A. HEATING MEASUREMENT SETUP

Fig. 7 shows the geometry of a small solid-state driven cavity used to measure the temperature change over time for different loadings. The cavity is cylindrical with a diameter

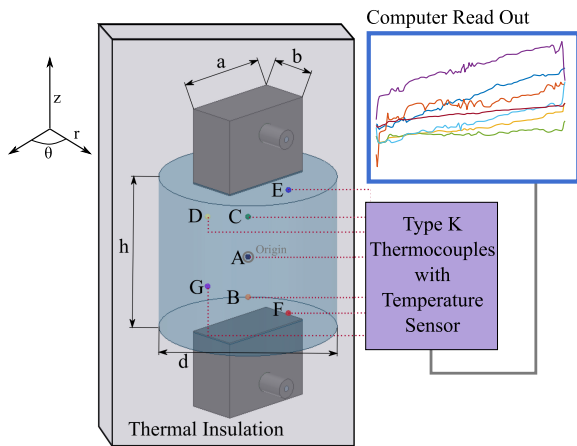


FIGURE 7. Geometry of the S-band waveguide probes and loaded cavity, with $d = 12.5$ cm, $h = 11.2$ cm, $a = 7.2$ cm and $b = 3.6$ cm. Two probes and placed on the bases of the cylinder. If only one probe is used (top probe in Fig. 8), the other is shorted with a metal sheet. In the experiments, seven small temperature sensors (not to scale here) are placed throughout the cavity at 7 fixed positions for all experiments.

TABLE 2. Table of Thermocouple Locations Referenced to the Center of the Cavity

Thermocouple	r (cm)	ϕ ($^\circ$)	z (cm)
A	0	N/A	0
B	0	N/A	-3.5
C	0	N/A	3.5
D	4	0	4
E	4	180	4
F	4	90	-4
G	4	270	-4

$d = 12.5$ cm and $h = 11.2$ cm in height, made of tin-plated steel. This 1.4ℓ “waste basket” models an appliance for personal use. The temperature is monitored with 7 type-K thermocouples placed at locations shown in Fig. 7 with thermocouple positions given in Table 2. The temperature is recorded using a Picolog6 module. The cavity is surrounded by thermal insulation consisting of 2.75 cm thick R5 foam, measuring 40 cm \times 32 cm \times 40 cm, with a reflective sheet on the internal surface. Solid-state GaN power amplifiers (PAs) are connected with coaxial-to-waveguide adaptors to the WR-340 (2.2–3.3 GHz) waveguide feeds.

Two setups are used to investigate heating, shown in Fig. 8. The first is a single-feed set of experiments with either one PA or two PAs connected to the top waveguide feed (Fig. 8(a)). The two PAs can be combined with a 0.67-dB loss coupler to approximately double the input power. For different cavity loadings, the impedance at the feed will be different, and the reflected power is dissipated in a set of attenuators with 50 dB loss before input to a power meter used to measure the reflected power. A tuner is added in some of the measurement to show a path for improving overall efficiency over time. Additional couplers and power meters are used to monitor the

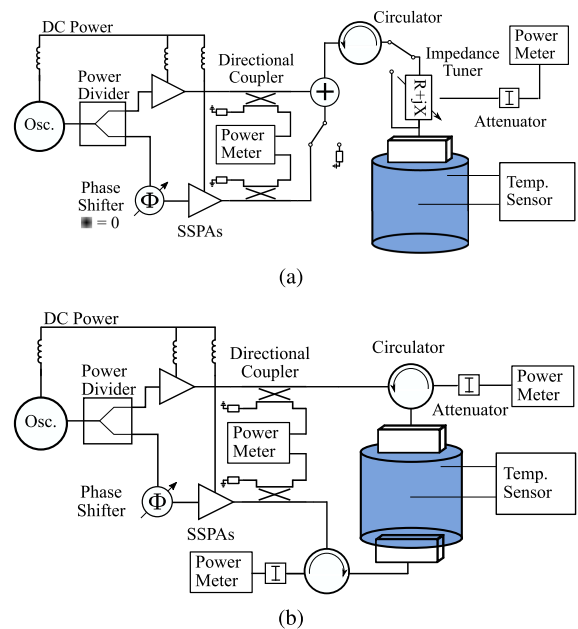


FIGURE 8. Two schematics of microwave reactors fed by solid-state power amplifiers (SSPAs) showing the different configurations compared in this investigation. Input power is measured through directional couplers positioned after the SSPAs. (a) One or two SSPAs power combine in phase and the combined power is fed through a single waveguide probe to the cavity. There is an option to feed the waveguide through a circulator to measure reflected power or through a load tuner to form a better match. (b) Two SSPAs are spatially combined in the cavity loaded with waste. The phase shift Φ is adjusted for improved heating uniformity.

output of the PAs. A power divider at the PA inputs is followed by a phase shifter in one of the branches to provide relative phase shift between the PA outputs. The phase shift is set to $\Phi = 0^\circ$ when a single waveguide feed is used as the cavity excitation.

Fig. 8(b) shows the setup for a dual cavity excitation where the relative phase shift Φ can vary. In this case, the output power of the two PAs is spatially combined in the waste loading. Otherwise, the setup is similar to the single-feed case. This setup allows an investigation of spatial power combining and a comparison to cases described in Fig. 8(a). The power delivered to the cavity is controlled through driver amplifiers in each path (not shown in the figures).

Two single-stage GaN hybrid PAs with Qorvo 70-W QPD1015 L packaged devices are designed, starting from load and source-pull simulations at the fundamental and second harmonic. The package capacitance presents a short at the third harmonic, limiting the waveshaping capability. The input is matched to a simulated large-signal reflection coefficient at 2.45 GHz, and the output match is designed to maximize output power while maintaining high PAE. The bias circuits present opens at the fundamental, and the second harmonic is shorted at the output of the device. The circuit is implemented on a Rogers 4360 G 32-mil thick substrate with the device mounted directly on the grounded heat sink, as shown in Fig. 9. The measured output power, PAE and gain vs. input power at 2.4 and 2.45 GHz are shown in Fig. 9. The output

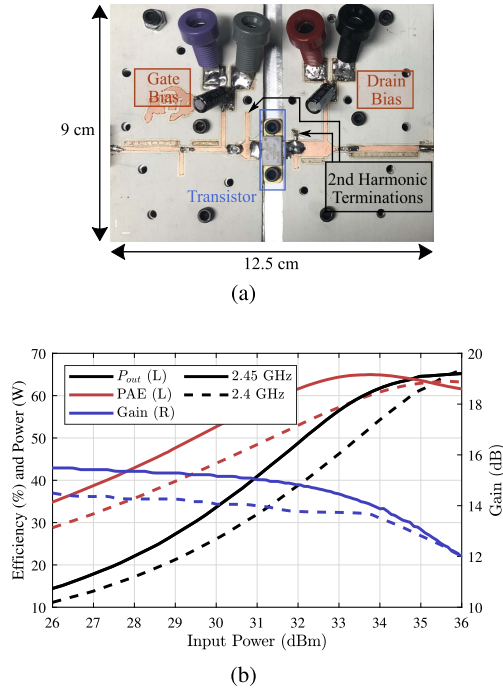


FIGURE 9. (a) Photograph of 70-W peak power GaN hybrid power amplifier showing the second harmonic termination. (b) Measured PA performance at 2.40 and 2.45 GHz with photograph of one of the two hybrid SSPAs based on a 70-W packaged GaN transistor. The input reflection coefficient is below -15 dB at both frequencies.

power and efficiency remain above 60 W and 52% for the 2.3–2.6 GHz (12%) bandwidth, allowing for broadband frequency modulation. Two power amplifiers are fabricated and have repeatable performance.

The following cases of loading and amplifier configurations are compared experimentally:

- A) Single power amplifier (PA) with $P_{OUT} = 70$ W. Since the reflection coefficient varies for different cavity loadings, we correct for this by keeping the delivered power constant at $P_{DEL} = 35$ W. Note that the paper and meat (hotdog) cavity fillings result in a mismatch at the probe with $\Gamma \approx 0.5$.
- B) Two equal 70 W PAs, externally combined with a power combining efficiency of 85.6%, delivering power to the cavity through a single probe. The changes in the reflection coefficient are compensated and the delivered power is kept constant at $P_{DEL} = 70$ W.
- C) Single probe with two PAs, same as case B, but with an added impedance tuner, Fig. 8(a). The power is adjusted to a level that allows fair comparison to other cases.
- D) Two equal 70 W PAs, each feeding a probe, spatially combined inside the waste volume, where P_{DEL} varies. The applied power is kept the same as in case B, for a fair comparison.

B. MULTIPHYSICS SIMULATIONS OF TEMPERATURE EVOLUTION

To investigate heating in simulations, the electric field distribution, and therefore Joule loss density, can be determined

TABLE 3. Table of Temperature Dependent Material Properties Used for Multiphysics Simulations [35], [36], [37], [38]

Temp. [$^{\circ}$ C]	ϵ_r	σ [$\frac{mS}{m}$]	c [$\frac{kJ}{Kkg}$]	ρ [$\frac{kg}{m^3}$]	κ [$\frac{W}{Km}$]
Paper Loading					
25	2.2	24.0	1.336	100	0.049
45	2.3	25.1	1.336	100	0.051
70	2.4	32.6	1.336	100	0.053
90	2.6	31.8	1.336	100	0.055
Bread Loading					
25	3.1	50	2.6	200	0.1
40	3.2	55	2.6	200	0.15
55	3.3	70	2.6	200	0.2
70	3.5	80	2.6	200	0.25
85	4.1	105	2.6	200	0.3
Meat Loading					
15	55	2315	3.5	1060	0.41
25	54.5	2246	3.5	1060	0.43
35	54	2466	3.5	1060	0.488
45	53	2287	3.5	1060	0.5
55	51	2328	3.5	1060	0.6
65	51	2519	3.5	1060	0.7

through full-wave electromagnetic simulations, and used in above equations to solve for the thermal evolution. However, this approach does not take temperature dependent material properties into account [29]. Measurements at 2.45 GHz of both inorganic [30] and organic materials often show changes in relative permittivity and conductivity with increasing temperature. The relative permittivity of meat [27] has been measured to drop from 62 to 58 when temperature increases from 15 $^{\circ}$ C to 55 $^{\circ}$ C. The conductivity increases (less than 5%) above about 25 $^{\circ}$ C.

A multiphysics approach which couples electromagnetic and thermal simulations is required to gain insight into the efficiency of heating and for improved cavity and probe design. This can be addressed using the 3D Finite-Difference Time-Domain (FDTD) technique for substances with temperature-dependent electromagnetic and thermal material parameters following the approach outlined in Table 3. The EM and thermal solvers operate as parts of an iterative procedure in which a steady state solution of the EM problem becomes an input for the thermal simulator, which then computes the temperature field induced after a pre-set heating time step. After each iteration, material parameters are upgraded in every cell of the FDTD mesh in accordance with the output temperature field from the thermal solver. This algorithm implemented in the 3D FDTD simulator QuickWave [28] allows for determining the time evolution of the 3D temperature distribution. Examples of simulations of the heating processes are reported in [31], [32], [33], [34].

To include the time evolution of the temperature profile, multi-physics simulations are performed for all three loadings,

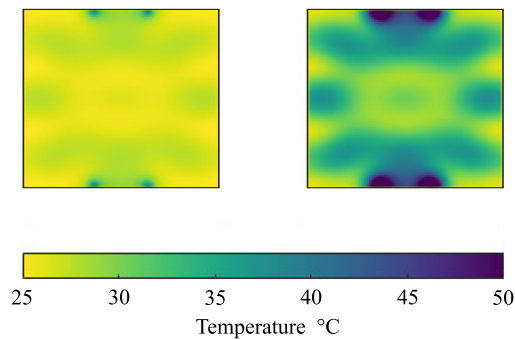


FIGURE 10. Simulated temperature distribution throughout the uniform bread loading at (a) the beginning of the heating process (after 20 s) with a maximum temperature of 25.2 °C, and (b) at after 100 s with a maximum temperature of 44.7 °C.

and are here shown for the case of bread in Fig. 10. The distribution looks similar to that of the volume power density, as expected, and at $t = 0$ agrees with the HFSS simulations from Fig. 5. In this case, the material parameters change is not sufficient to change the field distribution in the cavity.

To quantify the spatial temperature increase, we define *heating efficacy* e_H as the mean change in temperature over the volume and over the heating time Δt , normalized to the delivered power:

$$e_H = \frac{\mu_T}{\Delta t \cdot P_{DEL}}. \quad (6)$$

where μ_T is the mean of the temperature distribution and P_{DEL} is the power delivered to the cavity which takes into account any reflections as the loading changes. Another relevant metric is the one for uniformity of microwave heating throughout the volume. Here we adopt a definition for uniformity λ_p of dissipated power from [39]:

$$\lambda_p = \frac{\sigma_T}{\mu_T}, \quad (7)$$

where σ_T is the standard deviation of the temperature distribution in the entire volume.

To quantify the uniformity of heating, the heating efficacy (e_H) and power uniformity metric (λ_p) are calculated from coupled EM and thermal simulations for the three uniform loadings and are presented in Table 4. The efficacy does not change significantly for different excitations for the meat and bread loadings, but improves for the paper, while the uniformity improves for the meat and is phase-controllable for the bread loading.

V. EXPERIMENTAL RESULTS WITH HOMOGENEOUS WASTE MATERIALS

In this section, measurements with a single and two feeds for uniform paper, bread and meat loading are presented with the setups from Figs. 7 and 8 and compared with multiphysics simulations. The VSWR at the waveguide feed is measured for the three uniform loadings and is well matched for bread (VSWR < 2), but is poorly matched to the paper and meat

TABLE 4. Table Summarizing Two Probe Results

Test	Time(s)	e_H	λ_p
Paper Loading			
Circuit Combined	3	.124	.0475
Spatial Combined 0° phase	3	.1465	.2013
Spatial Combined 90° phase	3	.1419	.1555
Spatial Combined 180° phase	3	.138	.1256
Bread Loading			
Circuit Combined	78	.0056	.1717
Spatial Combined 0° phase	80	.0053	.1042
Spatial Combined 90° phase	80	.0053	.1484
Spatial Combined 180° phase	78	.0056	.2040
Meat Loading			
Circuit Combined	80	.0067	.0811
Spatial Combined 0° phase	100	.0001	.0176
Spatial Combined 90° phase	100	.0001	.0177
Spatial Combined 180° phase	100	.0001	.0179



FIGURE 11. Photograph showing the 1.4ℓ heating cavity with two waveguide feeds, and with 2.75-cm thick thermal insulation. Several photographs of different waste mixtures are also shown: (top) medium ϵ_r mixture; (center) paper loading; and (bottom) meat loading after 20 minutes of heating.

(hotdog) loading (VSWR > 5). For appropriate comparison, we keep the power delivered to the cavity constant, with input power equal to $P_{IN} = P_{DEL}/(1 - |S_{11}|^2)$. Next we describe results from measurements for cases A and B with a single probe for all three uniform loadings. The goal is to gain a better understanding of how the loss mechanisms change with increasing power level. Doubling the power should double the heating rate, however the loss mechanisms will differ between the two power levels because the material properties change with temperature. A photograph of the cavity with thermal insulation and a few material loadings is seen in Fig. 11.

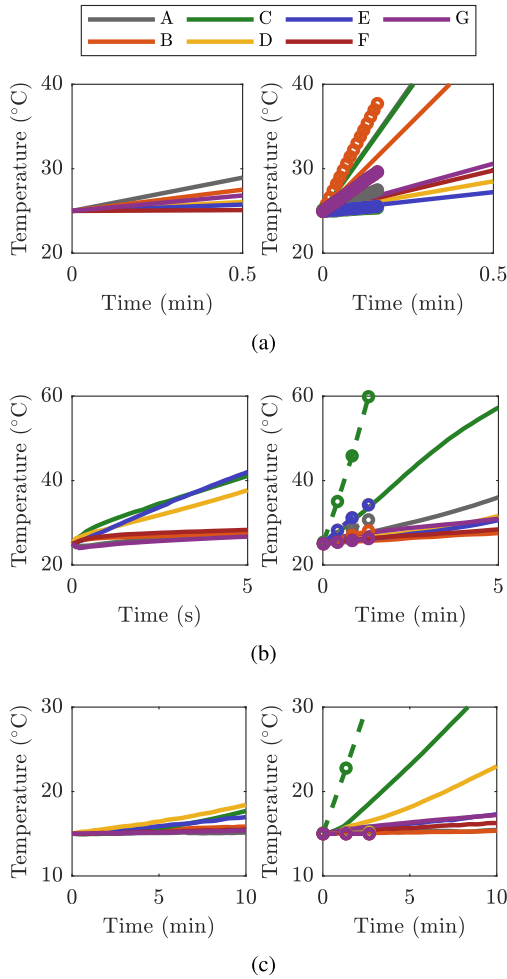


FIGURE 12. Measured temperature increase at 7 temperature sensor locations (A to G) for paper (a), bread (b), and meat (c) loadings of the cavity with a single feed for 35 W (left) and 70 W (right) of delivered power. The circular symbols show results from multi-physics simulations of heating rates at the thermocouple locations for the 70 W applied power.

A. SINGLE FEED WITH SINGLE PA

Fig. 12 show measured temperature time evolutions at the 7 thermocouple positions for the case of a single PA feed with a delivered power of 35 W (case A) on the left. For the paper loading, in 1 minute, the temperature increases up to 10 °C, while it takes more than 5 minutes for a comparable increase in temperature for the bread, and around 10 minutes for the meat loading. Although the delivered power is the same in all three cases, the meat takes a considerably longer time to heat up due to its relatively high specific heat and low thermal conductivity. For longer heating times, the slope changes due to material electrical property variations, as can be seen for the bread and meat loading.

B. POWER SCALING WITH SINGLE FEED

Next, the measurements are repeated with a two-fold increase in delivered power (case B), and the results are shown in Fig. 12 on the right. The circuit-combined measurements use a branch-line coupler to combine the 70 W amplifier outputs.

TABLE 5. Table of Single Port Measured VSWR

Material	Without Tuner	With Tuner
Paper	16	1.012
Bread	2.4	1.29
Meat	5.1	1.32

The theory (shown with circles) predicts the trends and is most accurate for the bread loading. Above 100 °C, limited information on food material electrical parameters exists, and therefore multiphysics simulations are performed in the lower temperature range to validate the trends. In all cases, the predicted temperatures are somewhat higher. The discrepancies are expected due to the following practical reasons: i) the material properties from the literature are validated with a simple and approximate loaded waveguide measurement [40]; ii) the multiphysics theory does not take into account the thermal losses (e.g. waveguide probe heating) that exist in the measurement.

The temperature measurements for the paper loading are sensitive to thermocouple placement around hot spots, which is reflected in the disagreement with simulations. In the case of meat loading, the measurements indicate that the thermal and electrical conductivities are different from the simulated ones. There is a visible tradeoff between the heating rate and uniformity described by the spread of temperatures across different thermocouples. When the power doubles, the heating rate does not double at every location. Instead, the temperature rates diverge and the hotter spots heat faster than the cold ones. The paper measurements are linear because the thermocouples are noisy over such short time periods and there is an initial temperature offset due to the high RF electric fields incident on the sensors. To compensate for this, temperature measurements immediately before and after the electric field is applied are used to create a linear approximation of the heating. This is not completely representative of the heating during operation, but shows the trends at different locations in the cavity. Although they have limited use in high electric fields, thermocouples offer a simple and cost-effective method for sampling the volumetric temperature distribution. An alternative method of temperature sensing that is not sensitive to high electric field strengths is infrared imaging, which only captures surface temperature.

C. SINGLE FEED WITH IMPEDANCE TUNER

Configuration C with a tuner to improve the delivered power is compared to the initial setup in Configuration A. The tuner is a mechanical single-slug tuner, consisting of an air coax with an adjustable parallel capacitance to ground. Table 5 shows the measured VSWR at the tuner input after adjusting the slug for best match for the three uniform loadings, compared to the impedance match without the tuner. Fig. 13 plots the measured temperature increase over time for probe C when the tuner is used for the three uniform loadings, showing increased

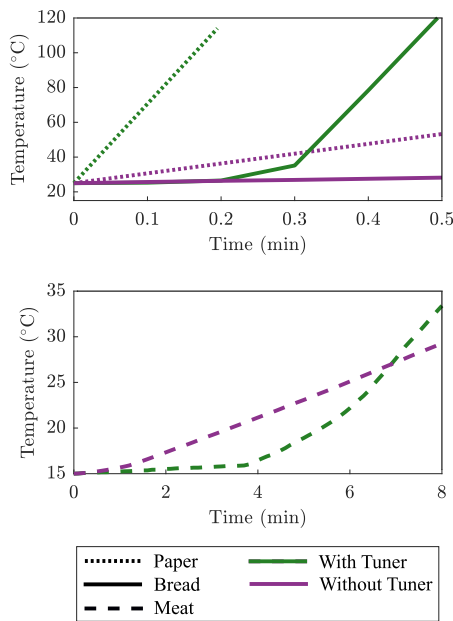


FIGURE 13. Measured temperature increase by temperature sensor C from Fig. 7, with and without a single tuner-matched feed for paper (dotted), bread (solid), and meat (dashed) loadings.

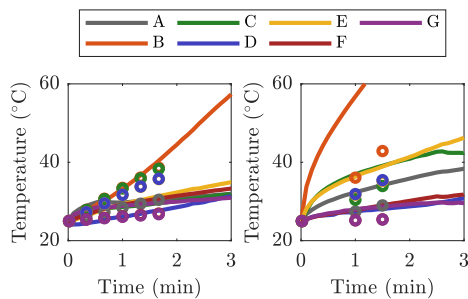


FIGURE 14. Measured temperature increase at 7 temperature sensor locations (A to G) for bread loading of the cavity with two feeds for 0° (left) and 180° (right) relative phase shift between the two probes. The symbols, 'o', show results from multi-physics simulations of heating rates at the thermocouple locations for the 70 W applied power.

heating for the matched case compared to case without the tuner. It is interesting to note that the relative increase in heating differs between materials, since their electrical properties change differently with temperature.

D. SPATIAL POWER COMBINING IN WASTE VOLUME

For the spatially combined method (case D), two 70 W amplifiers supply power to the two feed probes with circulators, depicted in Fig. 8(b). A phase shifter varies the relative phase between the two PAs between $\Phi = 0^\circ$ and $\Phi = 180^\circ$ in 45° steps. The thermocouple temperature sensor placement, data recording, and thermal insulation is the same as in the circuit-combined measurements.

Experimental validation for the trends shown in Table 4 was performed for bread loading. Fig. 14 shows heating results for 0° (left) and 180° (right) relative phase difference between the

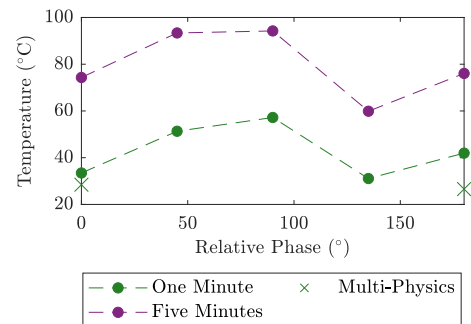


FIGURE 15. Readings at temperature sensor A after one minute and after five minutes of heating in two-port configuration. Measured temperature is plotted versus relative phase between ports. Multi-physics simulations done up to one minute are marked by X's.

two feeds. Measurements of heating rates at different points in the waste loading shows that the heating uniformity depends on relative phase between the two feeds. Additionally, controlling relative phase affects the electric field and therefore the heating distribution, shown at thermocouple A for several relative phase, Φ , settings in Fig. 15. The most important conclusions from this data are: (1) the heating uniformity can be improved by phasing between the two feeds; (2) for the high-conductivity meat loading the uniformity improves greatly with spatial power combining but not with relative phasing; and (3) the saturation in the temperature increases for the bread loading near 100°C indicating that the temperature dependence of the material properties affects heating for longer microwave powers or higher temperatures.

Another important result obtained from the multiphysics simulations is shown in Fig. 10, where the temperature distribution after 3 seconds is found for three relative phases (0° , 90° and 180°) and 35 W delivered power to each waveguide probe. (Note that in this case, the delivered power is difficult to measure.) These simulated results also show, in agreement with measurements, that phase shift can be used to control the heating patterns inside a loaded cavity.

When two feeds are used, the probe impedance changes due to near-field coupling. For the case of bread loading, the VSWR remains between 2.4 and 3 for all values of relative phase angle $\Phi = (0^\circ, 360^\circ)$ and for spatial rotations between the probes of $\theta = 0^\circ, 45^\circ$ and 90° . The mismatch for the meat loading is high, with a VSWR = 5, independent of phase shift or orientation, due the high absorption of meat that prevents coupling. For the case of paper loading, the coupling between the probes is high and changing the relative phase and/or orientation has a dramatic effect on the impedance match, with a minimum VSWR = 2.5 at ($\Phi = 260^\circ, \theta = 45^\circ$) and maximum VSWR > 10.

It was also found that with the meat loading the thermal properties change as the material heats up and the return loss improves drastically, from 5 to 25 dB (in this case, for 120 W applied power) and 5 to 10 dB (for 60 W applied power) over a 40 minute test. This supports the previously made claim that modeling the electrical parameters as a function of

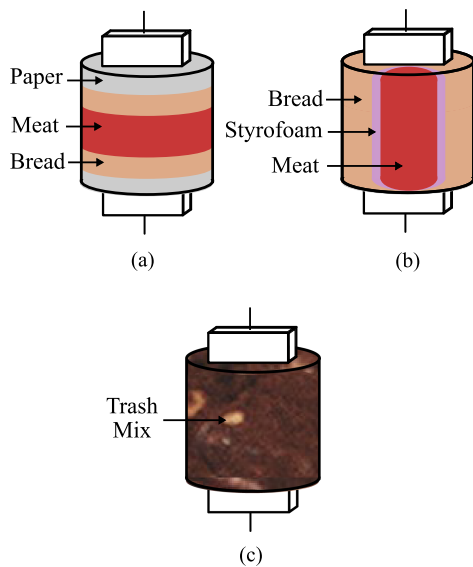


FIGURE 16. Geometry of experiments with multiple waste loading of the 1.4t cavity. (a) Vertical layering, with 19 mm of paper, 19 mm of bread, 36 mm of meat, 19 mm of bread, and 19 mm of paper, from top to bottom. (b) Radial layering with 3.2 mm of meat surrounded by 3 mm of bread loading. The meat and bread are separated with a thin Styrofoam ($\epsilon_r \approx 1$) wall. (c) Blended food waste mixture.

temperature is needed to improve performance over time with impedance tuning.

VI. EXPERIMENTS WITH MIXED WASTE MATERIALS

The previous section describes simulated and measured heating of a uniformly-loaded cylindrical cavity, with power delivered from one or two SSPAs which can be driven with a variable relative phase. When mixed waste is introduced in the cavity, the mode distribution changes. To investigate the effects of nonuniform waste materials on heating, measurements are performed for three mixed food waste scenarios:

1. three materials (meat, bread, and paper) are layered in the z dimension, Fig. 16(a);
2. two materials (meat and bread) are layered radially Fig. 16(b); and
3. Various food waste mixtures, low ϵ_r (coffee grinds, paper, oats), medium ϵ_r (coffee grinds, paper, oats, bread), and high ϵ_r (paper, bread, meat), fully filling the cavity, Fig. 16(c).

The first two sets of measurements are performed with 120 W of total applied power (taking reflection into account), with a focus on comparing circuit-combined single-feed and spatially-combined dual-feed heating. Fig. 17(a) shows the results measured by thermocouples A (center) and D (top). These measurements show that the temperature at thermocouple D is heating faster with the circuit power combining and a single-probe feed than with dual-feed spatial combining. However, spatial combining heats the center portion of the waste volume significantly faster, as shown by the more uniform temperature in the center and top of the cavity (dashed lines in Fig. 17(a)). In the experiments, the order of layers is

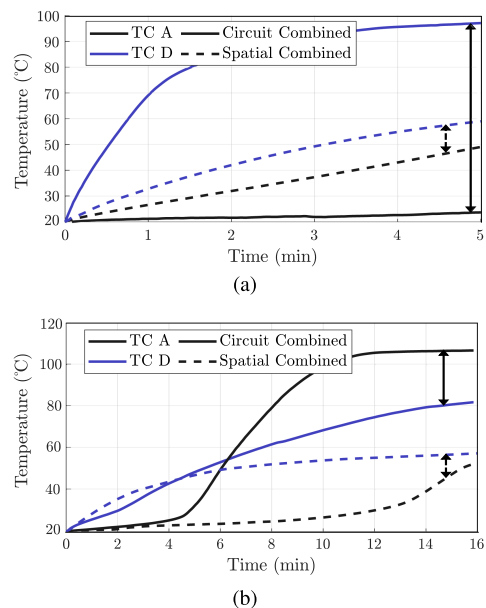
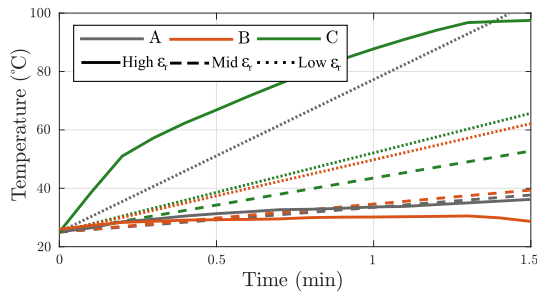


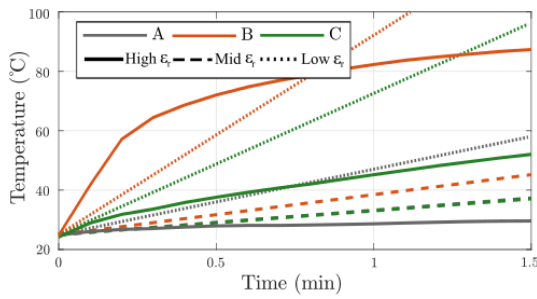
FIGURE 17. Measured temperature variation at thermocouples A and D of equal volumes of paper, bread, and meat loadings, layered vertically as described in Fig. 16(a) and radially as described in Fig. 16(b), with 120 W applied power to a single port by circuit-level combining of two PAs, and for the case when two probes are powered with 60 W applied power in each feed. The vertical arrows again show that the spatial combining provides significantly more uniform heating in this case.

chosen to provide a gradient of dielectric constants from lowest to highest, relative to the probe plane, in order to improve the penetration depth and the return loss. For a different layer structure (e.g. meat near the probe), the penetration depth would be reduced, limiting the advantage of spatial combining in this case. In summary, the spatial combining improves the heating uniformity. This is quantified by an approximately 70 °C difference between top and center of the cavity with a single feed, reduced to less than 10 °C difference for spatial combining after 5 min of heating with a total power of 120 W.

In the radially-distributed layers from Fig. 16(b), a thin Styrofoam separator surrounds the meat to prevent heat transfer between the two layers. Fig. 17(b) illustrates the importance of the temperature dependence of material properties. The center of the volume (thermocouple A) is heated with a delay for the circuit-combined compared to spatially-combined case, which indicates that the material properties are changing with temperature. The water content decreases with temperature, which increases penetration depth, resulting in a field distribution that changes faster for the circuit-combined measurement. It is also interesting that the temperature measured by thermocouple D flattens around 60° for the spatially-combined feeds. This saturation is likely caused by the power being concentrated away from the top of the cavity where thermocouple D is placed. For the radially non-uniform waste mixture, again the spatial combining results in better uniformity of about 10 °C vs. 30 °C difference between top and center of cavity after 15 min of heating with a total power of 120 W.



(a)



(b)

FIGURE 18. Measured temperature variation at thermocouples A, B, and C of equal volumes of a low, medium, and high dielectric constant mixed waste loadings. (a) Measurements with the impedance tuner at the single port for a delivered power of 129 W for each loading. (b) Measurement with two probes with relative phase adjusted to improve the match at the ports, with a delivered power of 90 W for the low and high permittivity mixed waste loadings and 100 W for the medium permittivity mixed waste. The total applied power is the same for (a) and (b).

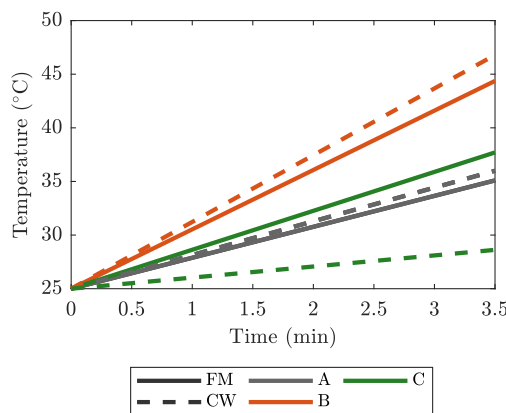


FIGURE 19. Measured temperature increase at the 3 thermocouple locations under a single probe with 60 W of applied power at 2.45 GHz (CW, dashed lines), and FM swept from 2.25 to 2.65 GHz (solid lines).

In the final case of mixed food waste, the cavity was filled with low, medium, and high permittivity mixtures. Two sets of measurements are presented: one with a single feed with an impedance tuner, and the other with two feeds and phase adjustment for best match. Due to the low permittivity and conductivity of the loading, the two feed probes couple and it is difficult to impedance match both simultaneously with a relative phase offset. The results of the measurements are shown in Fig. 18 for the two cases. Similar to the cases presented in

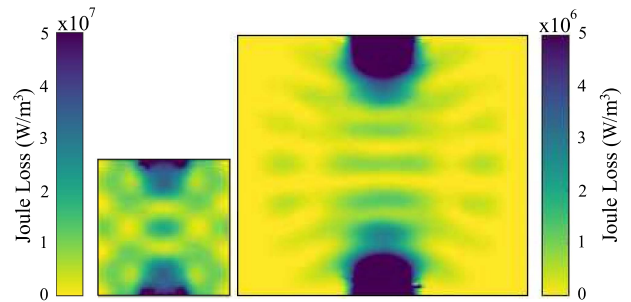


FIGURE 20. Simulated density of Joule losses through a central cross-section for 1.4ℓ (left) and 5.2ℓ (right) cavities with the same two waveguide feeds, with applied power scaled with volume (a factor of 3.7).

Fig. 17, spatial power combining demonstrates better heating uniformity compared with a single-port excitation. The exception is the low-permittivity mixture case, expected due to the stronger coupling between feed ports.

VII. CONCLUSION

In summary, this paper presents an investigation of a scalable microwave heating cavity for food waste pyrolytic breakdown, using circuit-level and spatial solid-state GaN power amplifier combining in the 2.45 GHz ISM band. The food waste materials chosen for the study have widely varying electrical conductivities and permittivities, that also vary with temperature, making multiphysics modeling essential for trend prediction. The experiments are performed in a 1.4ℓ cavity by combining two 70 W PAs with PAE > 60%, and the temperature is measured in 7 discrete locations throughout the volume using small thermocouples which minimally interact with the measurement. Three different uniform materials are used in the experiments and simulations, with complete cavity filling: paper, bread and meat (hotdog), due to their significantly varying electrical and thermal properties. Preliminary studies of frequency modulation and power scaling demonstrate some advantages of solid-state power generation, though further experimentation is needed.

One benefit of using solid-state sources over magnetrons is the ability to modulate the frequency. Fig. 19 shows the improvement in uniformity when a frequency-modulated (FM) excitation is used for paper loading, compared to the CW measurements. With 60 W of applied power, and a frequency swept linearly from 2.25 to 2.65 GHz over a 100 msec time period (a 16% modulation bandwidth), the FM measurements show a variation of about 10° after 3 minutes of heating, while the CW measurements show over 15° of variation throughout the volume.

Additionally, scaling of the cavity is investigated through simulations for a 5.2ℓ nearly cylindrical cavity made of the same material. For uniform bread loading, and the same type of waveguide feed, the field profile is different since different modes are excited. This results in density of Joule losses as shown in Fig. 20, which reveals the different modal content.

Some interesting conclusions are as follows.

- The results show that spatial combining within the waste volume has advantages in terms of efficacy, especially when uniform waste heating is desired.
- Controlling the relative phase between two or more power sources allows improved heating, which can improve heating when material properties vary with temperature.
- Simulations using FEM modeling of the cavity predict the modal content and Joule volume losses, while multi-physics FDTD modeling with temperature-dependent material properties are able to predict the volumetric temperature distribution and its evolution in time.
- Varying material properties change the matching conditions and coupling between the SSPAs, indicating that some tuning mechanism is beneficial, as shown with an impedance tuner and with a variable relative phase.
- Experiments with mixed waste materials show more uniform heating with volumetric power combining.
- Wideband frequency modulation enabled by solid-state sources shows increased heating uniformity.
- Increasing the cavity volume results in a different field distribution and different heating patterns when input power is scaled with volume.

In the experiments presented throughout the paper, after 40 minutes of heating with 120 W of applied microwave power, the reactor reduced mixed meat product to coke (coal). Since the reflection coefficient changes as the waste is heated, the energy efficiency calculation is not straightforward, and using the applied energy of 288 kJ gives the worst-case energy recovery ratio. Assuming coal has a calorific value of 30 MJ/kg, with 0.2 kg of resulting coal, 20 MJ is recovered for each MJ of microwave energy. The system efficiency is of course below unity, since the initial waste has energy content and the microwave generation is at most 70% efficient. The results shown in this paper suggest that solid-state amplifier combining can be efficiently used for waste material pyrolysis. Although demonstrated on a small 1.4ℓ cavity with modest 70-W PAs, the approach is scalable to larger volumes, power levels, as well as number of feeds. For larger volumes, a lower frequency (915 MHz) would be desirable due to the available high-power transistors and increased penetration depth in most materials of interest.

ACKNOWLEDGMENT

Z. Popović is grateful for support under a Lockheed Martin Endowed Chair of RF Engineering at the University of Colorado. The authors would like to thank Dr. Patrick Bluem (now at Lincoln Laboratory) and Kevin Stern at Worcester Polytechnic Institute for many helpful discussions and help with simulations and measurements.

REFERENCES

- [1] U.S. Environmental Protection Agency (EPA), “National overview: Facts and figures on materials, wastes and recycling,” Mar. 2020. [Online]. Available: <https://www.epa.gov/facts-and-figures-about-materials-waste-and-recycling/national-overview-facts-and-figures-materials#NationalPicture>
- [2] M. Ives, “Recyclers cringe as Southeast Asia says it’s sick of the West’s trash,” *New York Times*, Jun. 2019. [Online]. Available: <https://www.nytimes.com/2019/06/07/world/asia/asia-trash.html>
- [3] R. H. T. Edgington, “Recycling: Where is the plastic waste mountain?,” *BBC*, Jan. 2019. [Online]. Available: <https://www.bbc.com/news/science-environment-46566795>
- [4] J. J. Valdes and J. Warner, “Tactical garbage to energy refinery,” in *Sustainable Biotechnology*. Berlin, Germany: Springer, Jan. 2009, pp. 83–103.
- [5] J. C. Solarte-Toro, Y. Chacón-Pérez, and C. A. Cardona-Alzate, “Evaluation of biogas and syngas as energy vectors for heat and power generation using lignocellulosic biomass as raw material,” *Electron. J. Biotechnol.*, vol. 33, pp. 52–62, 2018.
- [6] A. L. Tasca, M. Puccini, R. Gori, I. Corsi, A. M. R. Galletti, and S. Vitolo, “Hydrothermal carbonization of sewage sludge: A critical analysis of process severity, hydrochar properties and environmental implications,” *Waste Manage.*, vol. 93, pp. 1–13, 2019.
- [7] D. Czajczyńska et al., “Potentials of pyrolysis processes in the waste management sector,” *Energy Procedia*, vol. 123, pp. 387–394, 2017.
- [8] Z. Wang, J. Cao, and J. Wang, “Pyrolytic characteristics of pine wood in a slowly heating and gas sweeping fixed-bed reactor,” *J. Anal. Appl. Pyrolysis*, vol. 84, no. 2, pp. 179–184, 2009.
- [9] A. Sarkar and R. Chowdhury, “Co-pyrolysis of paper waste and mustard press cake in a semi-batch pyrolyzer—optimization and bio-oil characterization,” *Int. J. Green Energy*, vol. 13, no. 4, pp. 373–382, 2014.
- [10] S. Barışçi and M. S. Öncel, “The disposal of combed cotton wastes by pyrolysis,” *Int. J. Green Energy*, vol. 11, no. 3, pp. 255–266, Mar. 2013.
- [11] S. A. Opatokun, V. Strezov, and T. Kan, “Product based evaluation of pyrolysis of food waste and its digestate,” *Energy*, vol. 92, pp. 349–354, 2015.
- [12] J. A. Onwudili, N. Insura, and P. T. Williams, “Composition of products from the pyrolysis of polyethylene and polystyrene in a closed batch reactor: Effects of temperature and residence time,” *J. Anal. Appl. Pyrolysis*, vol. 86, no. 2, pp. 293–303, 2009.
- [13] Y. Fernandez, A. Arenillas, and J. Angel, “Microwave heating applied to pyrolysis,” in *Advances in Induction and Microwave Heating of Mineral and Organic Materials*. Rijeka, Croatia: InTech, 2011, pp. 723–745.
- [14] H. B. Sharma, S. Panigrahi, and B. K. Dubey, “Hydrothermal carbonization of yard waste for solid bio-fuel production: Study on combustion kinetic, energy properties, grindability and flowability of hydrochar,” *Waste Manage.*, vol. 91, pp. 108–119, 2019.
- [15] C. Liu, H. Huang, Z. Liu, F. Huo, and K. Huang, “Experimental study on microwave power combining based on injection-locked 15-kw s-band continuous-wave magnetrons,” *IEEE Trans. Plasma Sci.*, vol. 44, no. 8, pp. 1291–1297, Aug. 2016.
- [16] “RF cooking with Goji,” 2023. [Online]. Available: <http://www.gojifoodsolutions.com/>
- [17] Z. Du et al., “Multi-physics modeling and process simulation for a frequency-shifted solid-state source microwave oven,” *IEEE Access*, vol. 7, pp. 184726–184733, 2019.
- [18] A. M. Paz, S. Trabelsi, S. O. Nelson, and E. Thorin, “Measurement of the dielectric properties of sawdust between 0.5 and 15 GHz,” *IEEE Trans. Instrum. Meas.*, vol. 60, no. 10, pp. 3384–3390, Oct. 2011.
- [19] S. Trabelsi, “Frequency and temperature dependence of dielectric properties of chicken meat,” in *Proc. IEEE Int. Instrum. Meas. Technol. Conf. Proc.*, 2012, pp. 1515–1518.
- [20] A. Reyes, M. Yarlequé, W. Castro, and S. Chuquizuta, “Determination of permittivity values using microwave dielectric spectroscopy for assessing apple and purple sweet potato quality parameters,” in *Proc. IEEE Int. Conf. Electromagn. Adv. Appl.*, 2018, pp. 593–596.
- [21] S. O. Nelson, “Dielectric spectroscopy of fresh fruit and vegetable tissues from 10 to 1800 MHz,” *J. Microw. Power Electromagn. Energy*, vol. 40, no. 1, pp. 31–47, 2005.
- [22] M. Sabet and H. Soleimani, “Mechanical and electrical properties of low density polyethylene filled with carbon nanotubes,” *IOP Conf. Ser., Mater. Sci. Eng.*, vol. 64, 2014, Art. no. 012001.
- [23] H. Saghlatoon, L. Sydanheimo, L. Ukkonen, and M. Tentzeris, “Optimization of inkjet printing of patch antennas on low-cost fibrous substrates,” *IEEE Antennas Wireless Propag. Lett.*, vol. 13, pp. 915–918, 2014.
- [24] J. Algie, “Dielectric constant and conductance changes in wool fibers produced by step changes in the relative humidity,” *Textile Res. J.*, vol. 34, no. 6, pp. 477–486, 1964.

- [25] American Society of Heating, Refrigerating and Air-Conditioning Engineers, "Thermal properties of foods," in *2006 ASHRAE Handbook-Refrigeration (SI)*. Washington, DC, USA: ASHRAE, 2006, ch. 9.
- [26] S. O. Keskin, S. O. Keskin, G. Sumnu, G. Sumnu, S. Sahin, and S. Sahin, "A study on the effects of different gums on dielectric properties and quality of breads baked in infrared-microwave combination oven," *Eur. Food Res. Technol.*, vol. 224, no. 3, pp. 329–334, 2007.
- [27] O. Sipahioglu, S. Barringer, and C. Bircan, "The dielectric properties of meats as a function of temperature and composition," *J. Microw. Power Electromagn. Energy*, vol. 38, no. 3, pp. 161–169, 2003.
- [28] "QuickWave," QWED Sp z o. o., Warsaw, Poland, 1998–2021. [Online]. Available: <http://www.qwed.eu/>
- [29] K. Halden, A. De Alwis, and P. Fryer, "Changes in the electrical conductivity of foods during ohmic heating," *Int. J. Food Sci. Technol.*, vol. 25, no. 1, pp. 9–25, 1990.
- [30] J. M. Catalá-Civera, A. J. Canós, P. Plaza-González, J. D. Gutiérrez, B. García-Baños, and F. L. Peñaranda-Foix, "Dynamic measurement of dielectric properties of materials at high temperature during microwave heating in a dual mode cylindrical cavity," *IEEE Trans. Microw. Theory Techn.*, vol. 63, no. 9, pp. 2905–2914, 2015.
- [31] E. M. Moon, C. Yang, and V. V. Yakovlev, "Microwave-induced temperature fields in cylindrical samples of graphite powder—Experimental and modeling studies," *Int. J. Heat Mass Transfer*, vol. 87, no. 8, pp. 359–368, 2015.
- [32] M. T. Porter, J. Binner, P. Kumi, K. E. Stern, and V. V. Yakovlev, "Computational characterization of microwave-enhanced CVI production of SiCf/SiC composites," in *Proc. 18th AMPERE Conf. Microw. High Freq. Heating*, 2021, pp. 48–55.
- [33] P. Kumi, S. A. Martín, V. V. Yakovlev, M. S. Hilario, B. W. Hoff, and I. M. Rittersdorf, "Electromagnetic-thermal model of a millimeter-wave heat exchanger based on an AlN: Mo susceptor," *COMPEL, Int. J. Computation Math Elect. Electron. Eng.*, vol. 39, no. 2, pp. 481–496, 2020.
- [34] C. M. Hogan, B. Hoff, I. Rittersdorf, and V. V. Yakovlev, "Computational characterization of a millimeter-wave heat exchangers with AlN:Mo susceptor of multiple cylindrical elements," *J. Microw. Power Electromagn. Energy*, vol. 56, no. 1, pp. 18–36, 2020.
- [35] T. V. Koutchma and V. V. Yakovlev, "Computer modeling of microwave heating processes for food preservation," in *Mathematical Modeling of Food Processing*, M. M. Farid Ed. Boca Ralton, FL, USA: CRC Press, 2010, pp. 625–658.
- [36] M. Celuch and P. Kopyt, "Modeling microwave heating in foods," in *Development of Packaging and Products for Use in Microwave Ovens*, M. W. Lorence and P. S. Pesheck, Eds. Sawston, U.K.: Woodhead Publishing, 2009, pp. 305–348.
- [37] V. V. Yakovlev, S. M. Allan, M. L. Fall, H. S. Shulman, and J. Tao, "Computational study of thermal runaway in microwave processing of zirconia," in *Proc. Microwave RF Power Appl.: 13th Int. Conf. Microw. Radio Freq. Heating*, 2011, pp. 303–306.
- [38] P. Kopyt and M. Celuch, "Coupled electromagnetic-thermodynamic simulations of microwave heating problems using the FDTD algorithm," *J. Microw. Power Electromagn. Energy*, vol. 41, no. 4, pp. 18–29, 2007.
- [39] P. Kumi and V. V. Yakovlev, "Computational procedure for quantitative characterization of uniformity of high frequency heating," in *Proc. 53rd IMPI's Microw. Power Symp.*, 2019, pp. 123–125.
- [40] Z. Abbas, R. Pollard, and R. Kelsall, "Complex permittivity measurements at Ka-band using rectangular dielectric waveguide," *IEEE Trans. Instrum. Meas.*, vol. 50, no. 5, pp. 1334–1342, Oct. 2001.



MEGAN C. ROBINSON (Student Member, IEEE) received the B.S. and M.S. degrees in electrical engineering from the University of Colorado, Boulder, CO, USA, in 2018 and 2020, respectively. She is currently working toward the Ph.D. degree from the same institution. She worked at Lockheed Martin Space Systems on RF test systems for JSAT-17 in 2017. Her research interests include high power amplifiers for biochemical applications and MMIC front ends for transceiver phased arrays. She was the 2022 recipient of a Department of Education GAANN fellowship.



JACK A. MOLLES (Student Member, IEEE) received the B.S. degree in physics from the University of California, Santa Barbara, CA, USA, in 2020, and the M.S. degree in electrical engineering from the University of Colorado, Boulder, CO, USA, in 2022. He is currently working toward the Ph.D. degree with the same university. His research focuses on high-power microwave solid-state circuits for a variety of applications, including RF heating and wireless power beaming.



VADIM V. YAKOVLEV (Senior Member, IEEE) received the M.Sc. degree in radio physics and electronics from Saratov State University, Saratov, Russia, in 1979, and the Ph.D. degree in radio physics from the Institute of Radio Engineering and Electronics (IRE), Russian Academy of Sciences (RAS), Moscow, Russia, in 1991. From 1984 to 1996, he was a Research Scientist with IRE, RAS. In 1993, he was a Visiting Researcher with the Centre Les Renardières, Electricité de France, Paris, France. In 1996, he joined the Department

of Mathematical Sciences, Worcester Polytechnic Institute (WPI), Worcester, MA, USA, as a North Atlantic Treaty Organization (NATO)/National Science Foundation (NSF) Fellow. He is with this Department and currently an Associate Research Professor. He is the Head of the Industrial Microwave Modeling Group, which he established in 1999, as a division of Center for Industrial Mathematics and Statistics, WPI. Funding sources of his research include the NSF, DoE, AFRL, AFOSR, and EADS (currently Airbus Group). His research interests include multiphysics modeling, microwave power engineering, non-distractive testing/imaging, and machine-learning optimization. Dr. Yakovlev is a Fellow of the International Microwave Power Institute (IMPI), a Member of the Association for Microwave Power in Europe for Research and Education (AMPERE), and a Member of the Massachusetts Institute of Technology (MIT) Electromagnetics Academy. In 2013 and 2022, he was the Chair of the Technical Program Committee for the 47th and 56th IMPI Microwave Power Symposia. From 2000 to 2016, he was the Founder of a series of international interdisciplinary seminars, Computer Modeling in Microwave Power Engineering, held annually. In 2007, he was the Guest Editor of the Special Issue on Modeling in Microwave Power Engineering of the *Journal of Microwave Power and Electromagnetic Energy*.



ZOJA POPOVIĆ (Fellow, IEEE) received the Dipl.Ing. degree from the University of Belgrade, Belgrade, Serbia, and the Ph.D. degree from the California Institute of Technology, Pasadena, CA, USA. She is currently a Distinguished Professor and the Lockheed Martin Endowed Chair of RF Engineering with the University of Colorado, Boulder, CO, USA. She was a Visiting Professor with the Technical University of Munich, Munich, Germany, from 2001 to 2003, and Institut Supérieur de l'Aéronautique et de l'Espace (ISAE), Toulouse, France, in 2014. She was the Chair of Excellence with the Carlos III University of Madrid, Getafe, Spain, in 2018 and 2019. Her research interests include high-efficiency power amplifiers and transmitters, microwave and millimeter-wave high-performance circuits for communications and radar, wireless powering, medical and industrial applications of microwaves, and microwave techniques applied to quantum sensing and metrology. She has graduated more than 70 Ph.D. students and currently advises 18 doctoral students. Dr. Popović was the recipient of two IEEE MTT-S Microwave Prizes for best journal papers, White House NSF Presidential Faculty Fellow Award, ASEE/HP Terman Medal, and the German Humboldt Research Award. She was the first woman to win the URSI Issac Koga Gold Medal in 1993, and was named the IEEE MTT Distinguished Educator in 2013 and the University of Colorado Distinguished Research Lecturer in 2015. Dr. Popović was elected as a Foreign Member of the Serbian Academy of Sciences and Arts in 2006 and a Member of the U.S. National Academy of Engineering in 2022. She is passionate about increasing the number of excellent women engineers and scientists, with eight women Ph.D. students currently in her group, with 66.7% retention rate in STEM.